Available online at www.sciencedirect.com
ScienceDirect
Journal of the European Ceramic Society 30 (2010) 3131–3136
www.elsevier.com/locate/jeurceramsoc

# Plasma sprayed $TiO_2$: The influence of power of an electric supply on particle parameters in the flight and character of sprayed coating

Pavel Ctibor*, Milan Hrabovský

*Institute of Plasma Physics, v.v.i., Academy of Science of the Czech Republic, Za Slovankou 3, 182 00, Praha 8, Czech Republic*

Received 25 November 2009; received in revised form 20 May 2010; accepted 29 May 2010
Available online 8 July 2010

**Abstract**

The influence of input power on sprayed powder and final coating was quantified for a water-stabilized plasma spray torch (WSP®) and ceramic coating formed from titanium dioxide ($TiO_2$). All other spray setup parameters were secured during the experiment with electric supply power as the only variable factor. In-flight particles were characterized by a Doppler particle velocimetry, the microstructure of the coatings was observed by microscopic techniques with computer image analysis, and phase composition was studied by X-ray diffraction. Various mechanical properties were measured – microhardness, surface roughness, and wear resistance in a slurry. Also other particular physical characteristics of the coatings – reflectivity and bandgap energy – were observed in their dependence on the supply power because they are associated with applications of the coatings. The higher the power the higher the coating quality will be: both its microstructure and mechanical performance. This substantial difference has the same trend for both power supplies utilized for the testing.


*Keywords:* Plasma spraying; DC plasma torch; Power supply; $TiO_2$; Wear testing; Bandgap

## 1. Introduction

In plasma spraying, electric power is one of the most important parameters controlling the product character.[1–3] By changing the quantity of heat available for plasma jet formation it is possible to change the quality of plasma sprayed coatings.[1] Particles of the feedstock powder attain a different degree of overheating and different kinetic energy for their movement towards the substrate when electric power is changed. This could be quantified by in-flight monitoring of the velocity, temperature and apparent diameter of the particles. Resulting coatings should exhibit different microstructure and properties, namely, mechanical ones.[1–4] Regarding the water-stabilized plasma spray torch the influence of power supply on produced coatings has never been systematically studied before.

Plasma sprayed coatings starting from $TiO_2$ feedstock powder usually consist of non-stoichiometric suboxides.[1,2,5] $TiO_2$ starts to lose oxygen at a temperature above 1600 °C in atmospheres. The partial pressure of oxygen required to reduce $TiO_2$ to $Ti_2O_3$, $Ti_3O_5$ or $Ti_4O_7$ is of the order of $10^{-5}$ Pa at around 2000 °C. During plasma spraying in the air, oxygen partial pressure does not go below 1 Pa. However, oxygen loss occurs resulting in the formation of non-stoichiometric titanium oxide. Oxygen deficient phases of $TiO_2$ (especially $Ti_3O_5$, $Ti_6O_{11}$) are sometimes observed in the coatings by XRD, namely, when the feedstock is an agglomerated titania nanopowder.[1] The loss of oxygen leads to the formation of titanium suboxides $TiO_x$. In the range $1.75 \leq x \leq 1.85$ (i.e., between $Ti_4O_7$ and $Ti_7O_{13}$) a homologous series (Magneli phases) of ordered structures with planar stacking faults exists.[5] The formation of non-stoichiometric and oxygen deficient lattice in rutile $TiO_2$ is due to the formation of structural defects.

This material is the subject of longstanding interest by the authors because of the variability of its promising properties – mechanical, namely, sliding and wear, as well as electrical and photocatalytic properties. Oxygen deficiency brings such a high variation in dielectric permittivity and the quality factor of titania, which facilitates studying it by a microwave microscopy.[6] Also Raman spectroscopy has been performed on a laser-treated surface and in reference to $Ti_4O_7$/$Ti_5O_9$ Magneli samples.[7] Low friction regimes were predicted near $TiO_{1.93}$ to $TiO_{1.98}$ and also near $TiO_{1.70}$.[8] The tendency of the rutile stoichiometry (ergo,

* Corresponding author. Tel.: +42 266053717; fax: +42 286586389.
*E-mail addresses:* ctibor@ipp.cas.cz, ctibor@ensil.unilim.fr (P. Ctibor).

0955-2219/$ – see front matter © 2010 Elsevier Ltd. All rights reserved.
doi:10.1016/j.jeurceramsoc.2010.05.029

the friction) to shift as a function of temperature and the partial pressure of oxygen triggers the thermo oxidative instability of this material.[9] A block-on-ring arrangement was used to study $Cr_3C_2$–NiCr coating against $TiO_2$ coating at different sliding speeds and loads.[10] The wear mechanism of the coating was explained in terms of the fatigue-induced detachment of a transferred $TiO_2$ layer at a lower load, plastic deformation, shear fracture and melting wear at a higher load.[11]

Regarding spraying by a water-stabilized plasma spray torch,[12] all properties of the $TiO_2$ coatings are controlled predominantly by microstructural features, such as porosity character, splat contact, cohesion and compactness. Physical properties are formidably influenced by an oxygen deficit in the coating whereas mechanical properties are rather weakly connected with them. Quantification of features taking place on the atomic level is difficult, first of all, because their influence on behavior of the material (plasma sprayed titania) is hidden behind the stronger effects of variations on the size level of an individual splat. These features include inter-splat contact, microcracks network, and quantity of spherical particles incorporated into lamellar coating due to premature solidification or improper melting of the feedstock. Overheating of the melt is in all cases high enough to transform anatase to rutile. $TiO_2$ is a material for which an ambient atmosphere must be considered as firmly reducing even when the melt is in contact with it for a very short time, such as during thermal spraying. So with plasma spraying of $TiO_2$, the phenomena are very complex: oxygen deficient stoichiometry is established within temperature window overlapping with the temperature window of phase (anatase to rutile) transformation, which takes place intrinsically.

Slurry abrasion resistance was of better quality for conventional coatings than for nanometric powder based ones; this conclusion has been confirmed by various WSP® samples.[12] Subtle differences in oxygen loss between micrometric and agglomerated nanometric powder seem to be responsible for it due to the possible origin of new share planes in the crystal lattice.

In the present paper spraying was done on two markedly different power levels, both with two diverse power generators. Various aspects of the results of the structural and physical as well as mechanical examination are discussed.

## 2. Experimental

### 2.1. Used power sources and feedstock powder

The plasma spraying experiments were performed by a direct current (DC) torch WSP®500 with electric arc stabilized by water vortex.[13] The torch could be operated at arc currents from 300 to 520 A, that is, arc power from less than 100 kW to more than 150 kW. Plasma in the jet is composed of oxygen and hydrogen and the torch is equipped by the external rotating disc anode. This WSP® torch exhibits extremely high power and plasma mass flow rate which enables also a high feed rate of the sprayed powder – on the order of tens of kilograms per hour.

Two types of power supply units were used in the experiments. The power supply PS1 was a classical thyristor controlled rectifier with the frequency of current ripple 300 Hz (Skoda, Czech Republic). The second power supply (PS2) was a high frequency converter type PL180WP (Bekaert Advanced Coatings Nv, Deinze, Belgium). Both of them were used for plasma spraying on two markedly different levels of electric current – 350 and 500 A. Corresponding powers were 100 and 150 kW, as previously noted. The crucial difference between both power sources was the frequency of a current ripple, which was 30 kHz for this second power supply. The amplitude of current fluctuations for both power supply units was similar.

Table 1
Parameters used for spraying.

| Parameter | Value |
|---|---|
| Feeding distance FD [mm] | 56 |
| Spray distance SD [mm] | 400 |
| Feeding nozzle diameter [mm] | 3 |
| Feeding gas | air |
| Powder size [μm] | 63–125 |

Plasma spraying of $TiO_2$ coatings was made with both power supplies at both arc powers. All spraying parameters and parameters of powder feeder as well as the movement of the plasma torch with respect to the substrate were the same for both power levels used. The details concerning spraying are summarized in Table 1.

As feedstock powder for spraying natural rutile $TiO_2$ sizes 63–125 μm (mean size 94 μm) was selected (ESAB Vamberk, Czech Republic). A chemical analysis of the feedstock powder discovered traces of copper and carbon as impurities. This particular form of $TiO_2$ is inexpensive and easy to feed into the plasma jet due to the compactness of its distinctive particles. The plasma spray feedstock was prepared by a conventional crushing and sieving processes. It is fed by compressed air into the plasma stream at a feeding distance (FD), which entraps it, melting and accelerating it towards the surface of the substrate, placed in a spray distance (SD) downstream.

The following parameters and characteristics were compared: velocity, temperature and diameter of particles traveling in the plasma jet (Table 2).

The efficiency of the deposition process $\eta$ (characterized by thickness $D$ of the coating), porosity $P$, roughness $R_a$ and $R_{y\,max}$, microhardness HVm, wear resistance in a Slurry Abrasion Response (SAR) test, reflectivity and bandgap energy.

### 2.2. Detail description of characterization techniques

In-flight particles were characterized by the Doppler Particle Velocimetry technique (DPV 2000, Tecnar Automation, St. Bruno, Canada). Measurements were carried out at spray distance, i.e., 400 mm from the nozzle exit. For each set of spray parameters, about 3000 particles were analysed and their average velocity, temperature and size were computed. The absolute errors on the temperature (grey body assumption) and velocity measurements were estimated at 100 °C and 10 m/s, respectively.

Porosity was determined on light microscopy images of cross-sections via image analysis software Lucia G (Laboratory

Table 2
In-flight particle parameters.

| Supply | PS1 | PS2 | PS1 | PS2 | PS1 | PS2 |
|---|---|---|---|---|---|---|
| Parameter | Velocity | Velocity | Temperature | Temperature | Diameter | Diameter |
| Unit | [m/s] | [m/s] | [°C] | [°C] | [μm] | [μm] |
| 100 kW | 43.7 | 41.5 | 2065 | 1858 | 90.1 | n.a. |
| 150 kW | 50.5 | 50.6 | 2078 | 1888 | 85.5 | n.a. |

Imaging, Praha, Czech Republic). Images were taken from 10 randomly selected areas for each sample, 250× magnification makes it possible to include objects larger than approximately 2 μm at the given resolution of a CCD chip. The precision of the measurement is influenced by a materialographic preparation of the cross-section and usually is considered to be 10%. In addition to simple quantification of porosity, other shape- and size-related factors of the coatings were also examined.

Microhardness of the coatings was measured by an optical microscope equipped with a Hanemann head (Carl Zeiss AG, Oberkochen, Germany) and the Vickers indenter by means of a 1 N load applied for a period of 15 s. The mean value of microhardness was calculated as an average from 20 indentations.

Surface roughness was determined by the apparatus Surtronic 3P (Taylor Hobson Ltd., Leicester, UK). Path length 25 mm was used on 5 assorted tracks, as parameters describing the surface $R_a$ and $R_{y\,max}$ were selected.

The SAR was measured by an approach based on the ASTM standard.[14] SAR is the mass loss (converted to volume loss) of standard-shaped samples when run for a period of time in a slurry. The block (substrate with coating, and coating towards the neoprene) was held by a constant force 22.2 N against a neoprene sheet that is mounted in a tray containing the slurry. The neoprene sheet acts as a lap. The tray is driven in a linear reciprocating motion, which keeps fresh slurry flowing under the block. The test is run for 9216 m in four increments with the mass loss being measured at the end of each increment after ultrasonic cleaning of samples.

All the coating weight losses were transformed to volume losses by applying densities measured by the Archimedean method – 4.2 g/cm$^3$. Finally the results are expressed in cubic millimeters per meter of the distance passed in the slurry. The accuracy of the measurement is approximately ±8%.

The X-ray diffractometer D 500 (Siemens AG, Berlin, Germany) with filtered Cu radiation was used for phase analysis. Angle $2\theta$ from 10° to 90° was recorded with a step 0.02°.

The diffuse reflectance of coatings was measured by a Scanning Spectrophotometer with a Multi-Purpose-Large Sample Compartment (Shimadzu Corporation, Kyoto, Japan). The reflectance curves, obtained between 250 and 2000 nm were than converted to absorbance and further recalculated[15] to allow an estimate of bandgap energy $E_{bg}$.

## 3. Results

### 3.1. Properties of particles in flight

The higher power produces higher velocity as well as a temperature of individual particles (for both supplies) whereas the corresponding apparent diameter of the particles is lower, Table 2. However the differences are not dramatic and these results should not be considered as absolute values but more as orientative values.

### 3.2. Properties of sprayed coatings

The thickness $D$ of coating was 1.20 mm at 100 kW and 1.96 mm at 150 kW, respectively. To obtain this thickness 40 passes of the torch with a speed of 300 mm/s were performed over a static substrate. The powder feed rate was fixed at 16 kg/h. Exactly the same procedure including the spray pattern and feeder setting was repeated for both power levels. In this way we can express the coating efficiency $\eta$ as the ratio of corresponding coating thicknesses (measured mechanically because coating was released from the planar substrate at cooling). Coating efficiency $\eta$ is therefore 52% for 100 kW if we consider 100% at 150 kW. This test was carried out using only the power supply PS1. We are referring here to relative efficiency; to bring absolute efficiency in terms of the ratio of the powder on input and powder embedded in a coating was not within the scope of this study and could be about 75% in reference to $TiO_2$. The rest includes evaporated matter and particles fed outside the plasma stream.

The bandgap energy estimation was based on absorbance measurement. Since the coating is thick and opaque, diffuse reflectance was measured, then converted to absorbance. Then bandgap transition energy was estimated at zero value of the Kubelka–Munk absorption coefficient $\alpha_{KM}$. This estimation was made for an indirect transition of an electron between two bands. The dependent variable parameter in this case is the root square of the product of $\alpha_{KM}$ and $E_{bg}$.[16] The values of all measured coating properties are summarized in Table 3.

## 4. Discussion

The particle velocity in plasma is higher when at a higher power, Table 2. The difference in temperature is not evident because of the great distance between the feeding point at FD (56 mm) and the SD measurement point (400 mm). The cooling is always rapid and the difference after traveling at 344 mm (i.e., SD minus FD) is nearly negligible. The apparent particle diameter is smaller for a higher power that corresponds to a slightly higher temperature. The decrease in the apparent diameter corresponds to higher evaporation on the surface of each individual particle at a higher power. But we must consider also a higher light intensity emitted by the plasma at a higher power and thereby possibly influencing the diameter measurement towards an overestimation. So the difference in impacting particle size for the two powers could be even higher than the measured data.

Table 3
Selected properties of the coatings.

| | PS1 (Skoda) | PS2 (Bekaert) | PS1 | PS2 |
|---|---|---|---|---|
| Parameter | Porosity | Porosity | Roughness $R_a$ | Roughness $R_a$ |
| Unit | % | % | μm | μm |
| 100 kW | 7.4 | 5.1 | 13.7 ± 0.6 | 15.3 ± 0.5 |
| 150 kW | 4.3 | 3.2 | 13.2 ± 1.2 | 13.5 ± 0.6 |
| Parameter | Microhardness | Microhardness | Roughness $R_{y\ max}$ | Roughness $R_{y\ max}$ |
| Unit | GPa | GPa | μm | μm |
| 100 kW | 9.2 ± 2.0 | 9.1 ± 1.5 | 108.9 ± 6.1 | 129.9 ± 11.0 |
| 150 kW | 12.0 ± 1.5 | 12.7 ± 1.2 | 119.2 ± 11.8 | 109.6 ± 9.3 |
| Parameter | SAR | SAR | $E_{bg}$ | $E_{bg}$ |
| Unit | $mm^3/m$ | $mm^3/m$ | eV | eV |
| 100 kW | 0.0273 | 0.0253 | 2.80 | 2.85 |
| 150 kW | 0.0157 | 0.0174 | 2.77 | 2.85 |

A single splat character is an important indication of suitability of the setup parameters for spraying of good quality coatings.[17] A comparison of typical splats is given in Fig. 1. In this case mirror-polished stainless steel is used instead of a sandblasted substrate. We see the circular shape at a higher power whereas at a lower power a complicated shape with central crater and many arms is formed. This corresponds typically to a worsened adhesion and cohesion of the sprayed material at a lower power.

Also the microstructures of the coatings, as given in Fig. 2, confirm that a lower power corresponds with structures having more pores and chaotic layout of the lamellas. Such features are very similar for both power supplies used.

The power 150 kW provides lower porosity for both supplies, Table 3. At the same time it gives higher circularity of pores together with a larger quantity of pores per $mm^2$, Fig. 3. In other words, pores are more globular without sharp edges and are finer, because porosity is lower for 150 kW than for 100 kW. These features have a crucial influence on mechanical properties.

Surface roughness is slightly higher at the lower power, which is associated with smaller in-flight particle velocity.

X-ray diffraction patterns of all coatings are practically the same. An example of it (PS1, 150 kW) is shown in Fig. 4. Besides characteristic peaks of rutile, weak reflections of anatase and Magneli phases (slabs with deficient oxygen stoichiometry, as indicated by M in Fig. 4) were also detected. The presence of anatase in the coatings sprayed from purely rutile feedstock powder is very similar to the phase composition changes described in Ref. 18 for the high velocity oxy-fuel spray technique. A certain loss of oxygen stoichiometry accompanies the phase changes, as expected.[12,18]

Optical properties of the coatings are presented in Fig. 5. Optical properties of anatase, rutile and amorphous phase $TiO_2$ thin films prepared by RF magnetron sputtering are summarized in Ref. 19. The analysis of optical absorption data for the anatase $TiO_2$ film shows an energy bandgap ($E_{bg}$) of 3.2 eV (extrapolation assumes indirect[16] transitions). On the other hand, the rutile $TiO_2$ film shows $E_{bg} \sim 2.9$ eV. The latter film also shows the presence of amorphous regions with $E_{bg} \sim 3.0$ eV.[16,19] The bandgap of both films, obtained using extrapolation assuming indirect transitions, has values slightly higher than our samples – plasma sprayed coatings, with bandgap energy 2.77–2.87 eV.

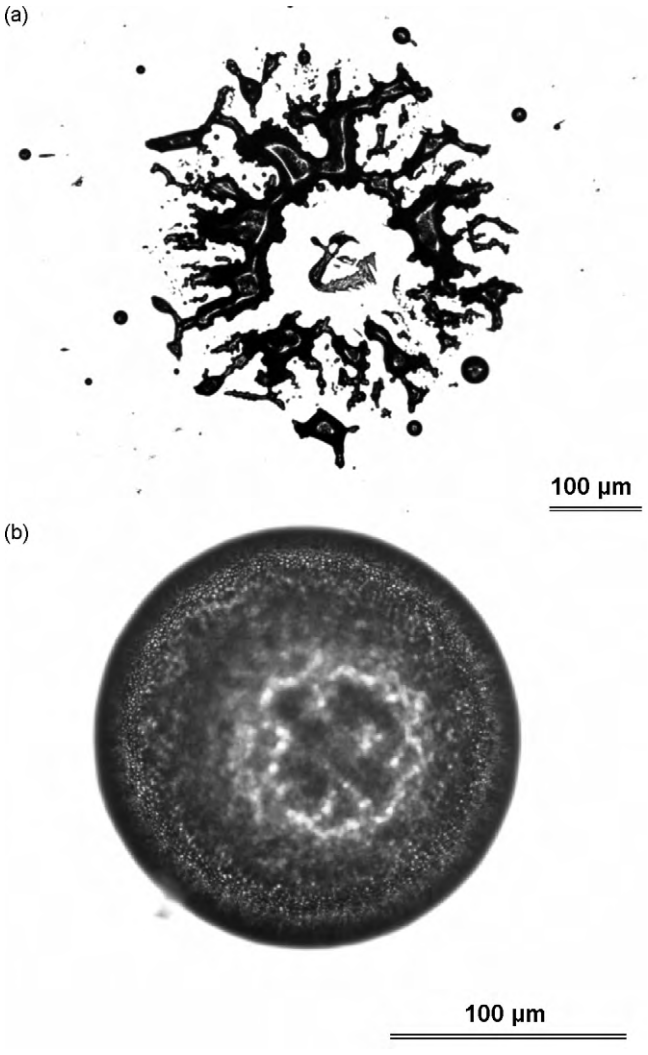


Fig. 1. Single splats produced by the source PS2 at 100 kW (top) and 150 kW (bottom).

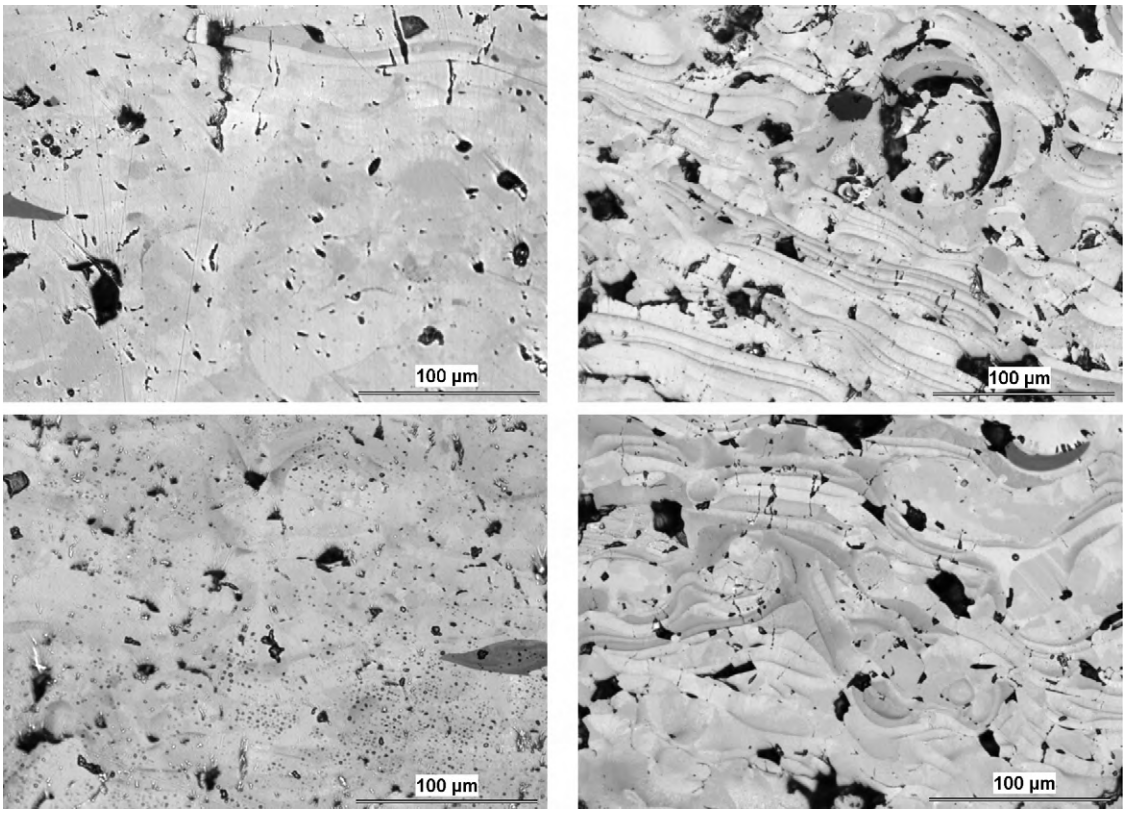


Fig. 2. Optical micrographs of cross-section of PS1 (top) and PS2 (bottom) coatings at 100 kW (left) and 150 kW (right).

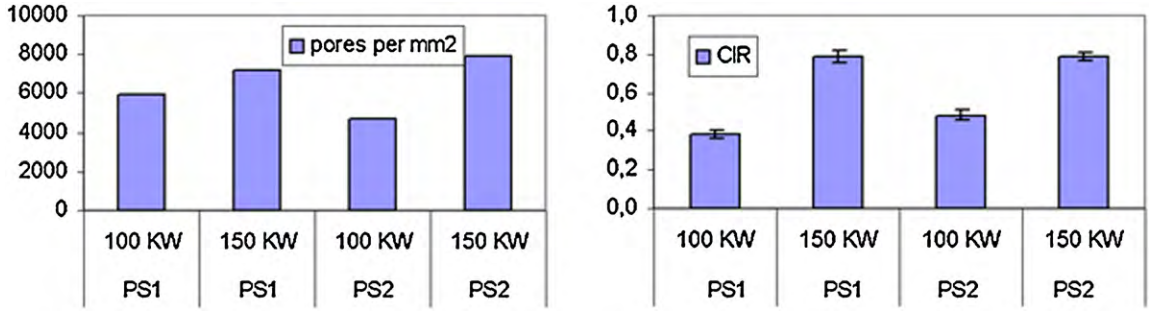


Fig. 3. Circularity (CIR) and number of pores per mm$^2$, determined by image analysis.

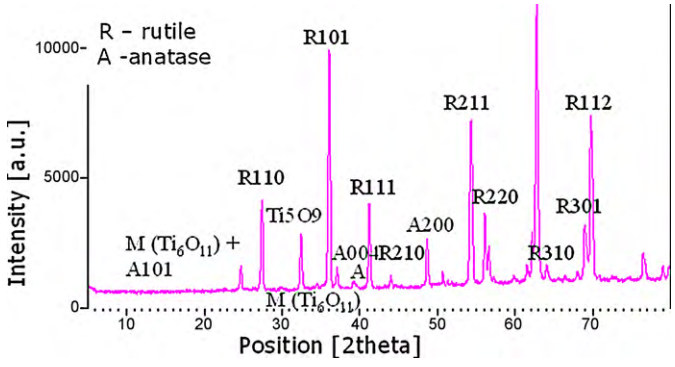


Fig. 4. X-ray diffraction pattern of the coating produced by the source PS1 at 150 kW.

Elsewhere[15] a dependence of the absorption coefficient $\alpha_{KM}$ on the wavelength is given for all three phases of $TiO_2$ (anatase, rutile and brookite). Rutile has markedly higher absorption in UV region. This higher absorption brings lower $E_{bg}$. This means that for excitation of the valence electrons to the conduction band, less energy is needed for plasma sprayed coatings in comparison with the mentioned films. This is making the plasma coatings studied here a prospect for photocatalytic application, similar to, e.g., alumina–titania coatings.[20] If we compare the two observed electric powers, there is an easier electron transition in the coatings sprayed with a higher power. It is consistent with other characteristics: warmer melt, higher impact kinetic energy which results in a lesser equilibrium state of the material in the coating.

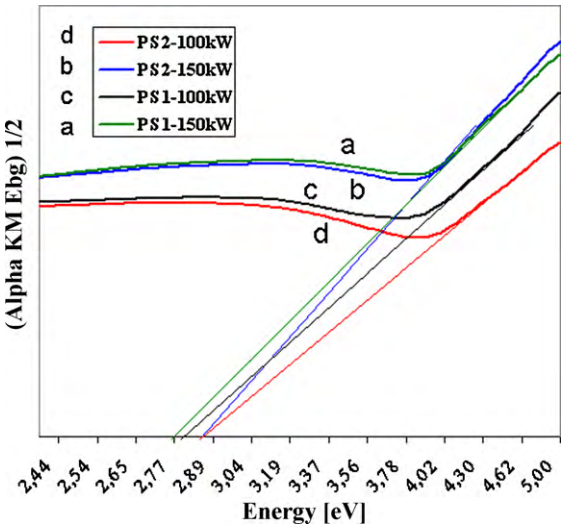


Fig. 5. Bandgap transition energy estimation from absorbance measurement.

## 5. Conclusions

The differences of properties of $TiO_2$ coatings deposited with the use of the two electric power levels were analyzed. A majority of important parameters of the particles and coatings exhibited marked changes in dependence on electric power. The higher the power the better the quality of the coating accompanied by its microstructure and mechanical performance. The two power supplies utilized for the testing exhibited this substantial difference and same trend.

The differences of the coatings sprayed with the different supplies were not significant. The spraying with high power (current) results in somewhat higher deposition efficiency, reduced porosity and higher wear resistance. This is attributed to the higher velocity of the in-flight particles in the plasma jet. Mechanical properties of WSP® sprayed coatings using natural $TiO_2$ as a feedstock are similar to those of coatings produced from synthetic $TiO_2$ agglomerated nanopowders.[12]

## Acknowledgements

The authors would like to acknowledge Dr. T. Chraska (IPP) for his assistance with DPV measurements. This work was supported by the Grant Agency of the Academy of Sciences of the Czech Republic (project no. IAAX00430803).

## References

1. Toma F-L, Bertrand G, Klein D, Meunier C, Begin S. Development of photocatalytic active $TiO_2$ surfaces by thermal spraying of nanopowders. *Journal of Nanomaterials* 2008 (article ID 384171).
2. Ramachandran K, Selvarajan V, Ananthapadmanabhan PV, Sreekumar KP. Microstructure, adhesion, microhardness, abrasive wear resistance and electrical resistivity of the plasma sprayed alumina and alumina–titania coatings. *Thin Solid Films* 1998;**315**:144–52.
3. Ageorges H, Vert R, Darut G, Zishuan F. Comparison of nanometric and micrometric alumina coatings on wear resistance. In: Marple BR, Hyland MM, Lau Y-C, Li C-J, Lima RS, Montavon G, editors. *Thermal Spray 2009: Proceedings of the International Thermal Spray Conference*. 2009. p. 1195–200.
4. Ageorges H, Ctibor P. Comparison of the structure and wear resistance of $Al_2O_3$–13 wt.% $TiO_2$ coatings made by GSP and WSP® plasma process with two different powders. *Surface and Coatings Technology* 2008;**202**:4362–8.
5. Berger L-M. Titanium oxide—new opportunities for an established coating material. In: Berndt C, editor. *Spray 2004: Advances in Technology and Application, Proceedings*. Osaka, Japan; 2004. p. 934–45.
6. Zhang Q, McGinn PJ. Imaging of oxide dielectrics by near-field microwave microscopy. *Journal of the European Ceramic Society* 2005;**25**:407–16.
7. Langlade C, Vannes B, Sarnet T, Autric M. Characterization of titanium oxide films with Magneli structure elaborated by a sol–gel route. *Applied Surface Science* 2002;**186**(1–4):145–9.
8. Gardos MN. Magnéli phases of anion-deficient rutile as lubricious oxides. Part I. Tribological behavior of single-crystal and polycrystalline rutile ($Ti_nO_{2n-1}$). *Tribology Letters* 2000;**8**(2–3):6665–78.
9. Guessasma S, Bounazef M, Nardin P, Sahraoui T. Wear behavior of alumina–titania coatings: analysis of process and parameters. *Ceramics International* 2006;**32**:13–9.
10. Li JF, Huang JQ, Zhang YF, Ding CX, Zhang PY. Friction and wear behaviour of plasma-sprayed $Cr_3C_2$–NiCr against $TiO_2$ coating under water- and ethanol-lubricated sliding. *Wear* 1998;**214**(2):202–6.
11. Li JF, Ding CX, Huang JQ, Zhang PY. Wear mechanism of plasma-sprayed $Cr_3C_2$–NiCr against $TiO_2$ coating. *Wear* 1997;**211**(2):177–84.
12. Ctibor P, Neufuss K, Stengl V. Structure and properties of plasma sprayed $TiO_2$ ceramics. In: Malik A, Rawat RJ, editors. *New nanotechniques*. Nova Science Publishers; 2009. p. 115–61.
13. Chraska P, Hrabovsky M. In: Berndt C, editor. *Proc. Int. Thermal Spray Conf. 1992*. 1992. p. 81–5.
14. Standard test method for determination of slurry abrasivity (Miller number) and slurry abrasion response of materials (SAR number), ASTM Designation. United States: G 75-95 ASTM; 1995.
15. Reyes-Coronado D, Rodríguez-Gattorno G, Espinosa-Pesqueira ME, Cab C, de Coss R, Oskam G. Phase-pure $TiO_2$ nanoparticles: anatase, brookite and rutile. *Nanotechnology* 2008;**19**:145–55.
16. Reddy MK, Manorama SV, Reddy AR. Bandgap studies on anatase titanium dioxide nanoparticles. *Materials Chemistry and Physics* 2002;**78**:239–45.
17. Fauchais P, Fukumoto M, Vardelle A, Vardelle M. Knowledge concerning splat formation: an invited review. *Journal of Thermal Spray Technology* 2004;**13**(3):337–60.
18. Lima RS, Moreau C, Garcia E, Miranzo P, Osendi MI. Development of HVOF-sprayed nanostructured $TiO_2$ coatings for high temperature applications. In: Lugscheider E, editor. *Thermal spray crossing borders—Proc. of the Intl. Thermal Spray Conf. 2008*. 2008. p. 774–8.
19. Naik VM, Haddad D, Naik R, Benci J, Auner GW. Optical properties of anatase, rutile and amorphous phases of $TiO_2$ thin films grown at room temperature by RF magnetron sputtering. In: *Proc. of the Materials Research Society fall meeting 2002, Symposium DD11.12*. 2002.
20. Stengl V, Ageorges H, Ctibor P, Murafa N. Atmospheric plasma sprayed (APS) coatings of $Al_2O_3$–$TiO_2$ system for photocatalytic application. *Photochemical and Photobiological Sciences* 2009;**8**:733–8.